



ORIGINAL ARTICLE

Exploration of the potentials of imidazole-based inhibitor package for heat exchanger-type stainless steel during acid cleaning operation



Ikenna B. Onyeachu ^{a,*}, Moses M. Solomon ^{b,*}, Kenneth K. Adama ^c,
Chukwuemeka F. Nnadozie ^d, Cornelius C. Ahanotu ^e, Christopher E. Akanazu ^f,
Demian I. Njoku ^{g,*}

^a Department of Industrial Chemistry, Edo State University Uzairue, P.M.B. 04 Auchi, Edo State, Nigeria

^b Department of Chemistry, College of Science and Technology, Covenant University, Canaanland, Km10, Idiroko Road, Ota, Ogun State, Nigeria

^c Department of Chemical Engineering, Edo State University Uzairue, P.M.B. 04 Auchi, Edo State, Nigeria

^d Department of Chemistry, Federal University of Technology Owerri, P.M.B. 1526 Owerri, Imo State, Nigeria

^e Department of Science Laboratory Technology, Imo State Polytechnic Umuagwo, Imo State, Nigeria

^f Department of Chemistry, Alvan Ikoku Federal College of Education, Owerri, Imo State, Nigeria

^g Department of Industrial Chemistry, Madonna University Nigeria, P.M.B 05 Elele, Rivers State, Nigeria

Received 27 January 2022; accepted 10 March 2022

Available online 14 March 2022

KEYWORDS

Acid cleaning;
Stainless steel;
Imidazole;
Cyclic voltammetry;
Corrosion inhibition

Abstract Protecting heat exchanger alloys from corrosion during acid cleaning is sacrosanct and necessitates the development and application of highly-efficient environmentally-friendly corrosion inhibitors. In the present work, gravimetry, electrochemical impedance spectroscopy (EIS), cyclic potentiodynamic polarization (CPDP), cyclic voltammetry and scanning electron microscopy-energy dispersive x-ray spectrophotometry (SEM-EDX) have been employed to investigate the potential of 1-benzylimidazole and its mixture with potassium iodide (KI) for the mitigation of stainless steel (SS316L) corrosion in 1 M HCl solution at 60 °C. After short immersion time, 1-benzylimidazole is found to decrease the weight loss and corrosion rate of the substrate and impacts an inhibition efficiency of $\approx 65\%$ at 2000 ppm dosage. The inhibitor adsorption followed the Freundlich isotherm. The synergism significantly lowers the rate of anodic half-reactions involving Fe and Cr oxidation which, in turn, boosts the inhibitor efficiency to $> 80\%$ through a competitive synergism. SEM-EDX characterization confirm that the passive layer formed in the presence

* Corresponding authors.

E-mail addresses: onyeachu.benedict@edouniversity.edu.ng (I.B. Onyeachu), moses.solomon@covenantuniversity.edu.ng (M.M. Solomon), demianifeanyi@gmail.com (D.I. Njoku).

Peer review under responsibility of King Saud University.



Production and hosting by Elsevier

of 1-benzylimidazole + KI significantly mitigated against the propagation of localized pitting corrosion. Prolonged immersion time, up to 72 h, lowers the inhibition efficiency of 1-benzylimidazole + KI mixture to 74 %.

© 2022 The Authors. Published by Elsevier B.V. on behalf of King Saud University. This is an open access article under the CC BY-NC-ND license (<http://creativecommons.org/licenses/by-nc-nd/4.0/>).

1. Introduction

Acid cleaning is a common industrial practice that is designed to remove inorganic scale deposits on surfaces of metallic equipment. For heat exchanger equipment, inorganic scales depreciate thermal conductivity and fluid-flow properties, and also initiate severe under-deposit corrosion that weakens the strength of the equipment (Obot et al., 2019; Malayeri and Jalalirad, 2014). During acid cleaning, dilute mineral acid (commonly HCl) is injected into the heat exchanger and allowed to reside there for some time at temperature up to 60 °C (Onyeachu and Solomon, 2020). Although this temperature facilitates the scale dissolution as soluble chlorides, simultaneous corrosion attack of the underlying substrate is also promoted. For heat exchanger alloys like stainless steel, which are traditionally-known for their remarkable corrosion resistance, this cleaning temperature and the aggressive chloride ions in the acid solution significantly negate passive film formation and stability (Obot et al., 2020; Yang et al., 2000). Conventionally, organic corrosion inhibitors have gained immense reputation as cheap and safe additives that can lower the rate of corrosion, when added to the acid cleaning solution. Nevertheless, elevated temperatures impact negatively on the performance of organic corrosion inhibitors leading to loss of efficiency (Onyeachu et al., 2020; Umoren et al., 2021; Iroha and Maduelosi, 2021; Solomon et al., 2021).

Since acid cleaning practice is inevitable in the industry, corrosion inhibitor addition is also an indispensable practice. The current global advocacy for greener and more environmentally-benign chemicals make it imperative to develop corrosion inhibitors that meet the high-efficiency and low-toxicity standards (as stipulated by PARCOM Protocols on Methods for the Testing of Chemicals Used in the Offshore Oil Industry, 2006). These standards are readily found among imidazole and its derivatives. They represent a class of non-toxic and cost-effective nitrogen-based heterocyclic compounds (Shalini et al., 2010). They serve as nuclei for the synthesis of a wide variety of pharmaceutical products (Ranjith, 2016; Narasimhan et al., 2011), and are key compounds applied in the advancement of green chemistry and organometallic catalysis (Balalaei and Arabanian, 2000; Keim, 2000). Very importantly, too, their corrosion inhibition properties have been reported for a variety of alloys in different corrosive environments (Obot et al., 2015; Zhang et al., 2009; Yan et al., 2020; Ko et al., 2021; Srivastava et al., 2021; Wang et al., 2018; Xiong et al., 2021; Eduok et al., 2018; Singh et al., 2017; Li et al., 2021; Zeng et al., 2021). Molecular structure influences their adsorption property; hence, simpler structures enjoy less-restrictions (during adsorption) due to reduced steric hindrances. In view of the aforementioned, and given the excellent corrosion inhibition efficiency it provided for steel in a typical acid corrosion environment (Onyeachu et al., 2021), we are motivated to investigate 1-benzylimidazole (and its mixture with potassium iodide, KI) as corrosion inhibitor for the protection of a heat exchanger stainless steel under acid cleaning conditions.

In 1-benzylimidazole, a phenylmethyl group is attached to the nitrogen atom in an imidazole ring, as elucidated in Fig. 1. Density functional theory calculations has shown that the imidazole nitrogen in 1-benzylimidazole is the electron-rich and principal adsorption site of the molecule on a steel surface in an acidic medium (Onyeachu et al., 2021). Its low energy band gap (ΔE) ensures an ease of electron release and acceptance; a prerequisite for good corrosion inhibition (Onyeachu et al., 2021). Its simple structure enables it to inherently orient in a near flat/parallel position during adsorption; a prerequisite for high interaction strength and surface coverage (Onyeachu et al., 2021).

The molecule is also a major pharmacological ingredient (Hachula et al., 2010; Khabnadideh et al., 2003) and exhibits $\text{Log } P_{o/w} = 1.93$ and $LD_{50} = 75 \text{ mg/kg}$, hence, is adjudged a low-toxic molecule by PARCOM standard (1-benzylimidazole, 2021). For carbon steel corroding in acidic solution (Onyeachu et al., 2021; Ismail et al., 2019); 1-benzylimidazole modified the electrochemistry by influencing more of the anodic (oxidation) arm of the potentiodynamic polarization curves. Such behaviour makes us suspect that its adsorption could also improve the oxidative reactions involving Fe, Cr and Ni in stainless steel, thereby, favouring the formation of highly-protective passive layers. When little quantity of potassium iodide (KI) is added as additive to the corrosion inhibitor, like is usually the case in many industrial corrosion inhibitor formulations, we further envisage a synergistic improvement in the action of 1-benzylimidazole. This is because iodide ions have the capacity to charge a metal surface negatively and promote the adsorption of positively-charged inhibitor molecules (Solomon et al., 2020; Umoren and Solomon, 2014), as 1-benzylimidazole would exist in an acid solution in protonated form (Onyeachu et al., 2021; Cardona et al., 2014). From an overall perspective, however, not much research works has investigated imidazole derivatives as inhibitors for the mitigation of the acid corrosion of stainless steel (Ribeiro et al., 2015; Moreira et al., 2014; Jia et al., 2013). Filling this research gap is important, especially at an elevated temperature, given the merits of such compounds.

Classical weight loss and the instrumental electrochemical techniques are some of the conventional corrosion testing techniques used in many industries. The ASTM G1-03 (ASTM-G 01-03, 1997) highlights the guidelines for performing weight loss experiments. The technique provides the merits of high accuracy, precision, reproducibility and minimal methodical errors (Daniyal and Akhtar, 2020). When performed over a given time, it can be used to deduce average corrosion rate (ASTM-G 01-03, 1997). Electrochemical impedance spectroscopy (EIS), cyclic voltammetry (CV) and potentiodynamic polarization (PDP) are some of the most important electrochemical techniques. EIS, a non-destructive technique, involves exciting the corroding metal with low-amplitude alternating-current potential in order to probe the corrosion resistance mechanism with respect to the solution dielectric properties (Daniyal and Akhtar, 2020). In the PDP technique, especially its cyclic derivative (cyclic potentiodynamic polarization, CPDP), rate and mechanism of electrochemical reactions at the corroding metal surface are deduced by impressing a wider range of direct-current potential perturbation. Kinetics and mechanism are interpreted from parameters like corrosion current density (i_{corr}) and corrosion potential (E_{corr}), and also from phenomena like active corrosion, passivation and passivation breakdown, and pitting corrosion (Daniyal and Akhtar, 2020). Furthermore, the CV technique is also a direct current polarization technique but involves perturbing the corroding metal with a cyclic potential scan and measuring the current flow. The resultant anodic and cathodic peaks in a cyclic voltammo-

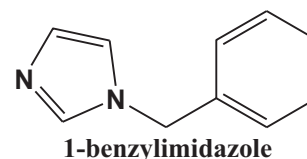


Fig. 1 Structure of 1-benzylimidazole.

gram can aid the identification of plausible corrosion products formed on the alloy surface during the corrosion process (Onyeachu et al., 2020; Elgrishi et al., 2018). Knowledge of this could provide reasonable explanations to the electrochemical mechanism controlling the corrosion process.

In the present research work, we apply weight loss experiments to screen the effect of concentration and KI addition on the inhibition performance of 1-benzylimidazole during corrosion of stainless steel SS316 L after immersion 1 M HCl solution at 60 °C. Using the optimized inhibitor concentrations derived from weight loss (without and with KI addition), we employ electrochemical measurements using EIS, CV and CPDP to interpret mechanism of the corrosion inhibition. Scanning electron microscopy (SEM) and energy dispersive x-ray spectrophotometry (EDX) were employed to probe the effect of the corrosion inhibitor system on the surface degradation of the stainless steel after corrosion. The effect of prolonged immersion time (72 h) was also considered.

2. Experimental section

2.1. Chemicals and materials

1-benzylimidazole and potassium iodide (KI) were purchased from Sigma Aldrich as analytical grade chemicals. Concentrated HCl (35%) and isopropanol were purchased from Fisher scientific. The acid solution (1 M HCl) was prepared by diluting the concentrated acid with distilled water. A stock solution of 1-benzylimidazole was prepared in isopropanol, from which inhibitor concentrations of 500, 1000, 1500 and 2000 ppm were prepared by diluting stock with the acid solution. The elemental composition of the stainless steel SS 316L has been reported previously (Obot et al., 2020). The alloy was cut into weight loss coupons with total exposed surface area of 22.73 cm² while the electrochemical coupons had 1 cm² surface area exposed for testing after cold mounting in epoxy resin. The surfaces of coupons were prepared by polishing with silicon-carbide papers having grit sizes 400, 600, 800 and 1000. They were subsequently washed thoroughly with running tap water, degreased with acetone, dried with warm air and used immediately. A thermostatic water bath was utilized to maintain a 60 °C temperature at which all corrosion measurements were performed.

2.2. Weight loss measurements

Preliminary weight loss experiment was performed for 6 h to screen the corrosion inhibitor and optimize concentration. Prolonged weight loss experiment, with optimized inhibitor concentration, was performed by immersing the alloy for 72 h in uninhibited and inhibited solutions. Duplicate stainless steel coupons were immersed in 200 mL of inhibited and uninhibited 1 M HCl solution at 60 °C. After each immersion time, the coupons were withdrawn from the solutions and cleaned according to ASTM G1-03 standard procedure (ASTM-G 01-03, 1997). The weight loss after immersion (ΔW) was calculated based on Eq. (1) from which the corrosion rate (v , mm/yr) was calculated according to Eq. (2); whereby ρ = density of the stainless steel sample (7.99 g cm⁻³), T = immersion time (6 h), and A = surface area of the coupons (22.73 cm²). The corrosion inhibition efficiency (% IE) deduced from weight loss measurement was calculated according to Eq. (3). The

effect of KI on the inhibitor performance was investigated in the acid solution without and with maximum inhibitor concentration.

$$\Delta W(g) = W_{(\text{beforeimmersion})} - W_{(\text{afterimmersion})} \quad (1)$$

$$v(\text{mm/yr}) = \frac{\Delta W \times 87600}{A \times \rho \times T} \quad (2)$$

$$\%IE = 1 - \frac{v_{(\text{withininhibitor})}}{v_{(\text{withoutinhibitor})}} \times 100\% \quad (3)$$

2.3. Electrochemical measurements

The electrochemical experiments were conducted with the lowest and maximum inhibitor concentration to interpret the mechanism of the inhibitor action without and with KI addition. The electrochemical experiments were performed in a 200 mL three-electrode system that consisted of Ag/AgCl (sat. 4.2 M KCl) as reference electrode, 3 cm × 3 cm Pt. sheet as the counter electrode and the stainless steel as working electrode. The measurement was conducted on a Gamry Potentiostat/Galvanostat/ZRA Reference 600 + workstation equipped with the Echem analyst software for the extrapolation of electrochemical parameters. All electrochemical tests commenced with an open circuit potential (OCP) determination during 1800 s of free corrosion in order to establish a steady-state condition which is imperative for every electrochemical corrosion measurement. At the OCP, electrochemical impedance spectroscopy (EIS) measurement was conducted, under potentiostatic mode, by applying an alternating-current signal with amplitude of 10 mV over a frequency range of 10⁵ Hz to 10⁰ Hz. Cyclic voltammetry measurements were carried out in the potential range of -0.6 V vs. Ag/AgCl to +0.6 V vs. Ag/AgCl using a sweep rate of 10 mV/s. Cyclic potentiodynamic polarization (CPDP) measurements were conducted using the following parameters: initial potential = -0.25 V/Ref; apex potential = 1 V/Ref; final potential = 0 V/Ref; forward and reverse scan rate = 0.5 mV/s. The efficiency of inhibition (% IE) was calculated from the EIS and CPDP results using Eqs. (4) and (5), respectively.

$$\%IE_{\text{EIS}} = 1 - \frac{R_{p(\text{withoutinhibitor})}}{R_{p(\text{withininhibitor})}} \times 100\% \quad (4)$$

$$\%IE_{\text{CPDP}} = 1 - \frac{i_{\text{corr}(\text{withininhibitor})}}{i_{\text{corr}(\text{withoutinhibitor})}} \times 100\% \quad (5)$$

2.4. SEM characterization

Scanning electron microscopy (SEM) was employed to peruse the surface morphology of the stainless steel after corrosion in the blank acid solution and in the acid solution containing the optimum inhibitor concentration + KI. The SEM was coupled with an energy dispersive x-ray spectrophotometer (EDX) to determine the elemental composition of the corrosion layer. The SEM experiment was conducted on a microscope JEOL JSM-6610 LV model operated at a voltage of 20 kV and irradiation current of 10 mA.

3. Results and discussion

3.1. Weight loss and corrosion rate results

The weight loss and corresponding corrosion rate recorded for SS 316L stainless steel after 6 h of immersion in 1 M HCl at 60 °C without and with different concentrations of 1-benzylimidazole are presented in Table 1. From the results obtained, the stainless steel experienced a concentration-dependent retardation in weight loss when 1-benzylimidazole was added to the acid solution. This retardation is even more pronounced with the addition of 1 mM KI. For instance, relative to a weight loss of 0.16 ± 0.014 g (12.87 ± 1.59 mm/yr) recorded for the substrate in the uninhibited HCl solution, a weight loss of 0.056 ± 0.007 g (4.90 ± 1.36 mm/yr) is observed in the presence of 2000 ppm of the inhibitor and represents a protection efficiency of approximately $65.12 \pm 1.87\%$. The addition of 1 mM KI to this inhibitor concentration further decreased the weight loss to 0.040 ± 0.004 (3.21 ± 0.46 mm/yr) and boosted the efficiency to approximately $75.03 \pm 0.44\%$. This phenomenon can be explained accordingly.

When immersed in the acid solution, the stainless steel acquires a potential that triggers dissolution of reactive metals, especially Fe and Cr, via some oxidation reactions (Strehblow, 2016; Maurice and Marcus, 2018). These oxidation reactions occur simultaneously with reduction reactions, the most important being the reduction of H^+ ions into $H_{2(g)}$. This dissolution causes the weight loss observed during the immersion experiment. Although corrosion-resistant oxides/hydroxides of Fe and Cr are the major products formed from this corrosion process (Strehblow, 2016; Maurice and Marcus, 2018), the stability of their passive film, at the working temperature, would surely be jeopardized by Cl^- ions in HCl (Marcus, 1998; Marcus et al., 2008). As a cationic inhibitor in an acid solution (Onyeachu et al., 2021; Cardona et al., 2014); 1-benzylimidazole could lower the extent of weight loss experienced by the alloy through adsorption and blocking of reactive sites to impede both oxidation and reduction reactions. Oxidation processes at anodic sites are blocked by electron transfer between the d-orbitals of Fe and Cr, and the electron-rich cen-

tres in 1-benzylimidazole, i.e. the nitrogen atoms and C=C pi-bonds. Given the cationic nature of 1-benzylimidazole in the acid solution, the blocking of oxidation processes could also be facilitated by pre-adsorbed anionic species, especially, chloride ions in the acid devoid of 1 mM KI. On the other hand, the reduction reaction is lowered by the preferential adsorption of 1-benzylimidazole cations, over H^+ ions, on the cathodic sites. Surely, the 1-benzylimidazole has a larger size than H^+ and, therefore, would cover larger cathodic surface area. Once adsorbed, the inhibitor molecules can link up and spread into a continuous protective layer, as determined by the surface microstructural characteristics of the alloy. The equation $\theta\{0 \leq \theta \leq 1\} = \frac{\%IE}{100}$ relates corrosion inhibition efficiency (% IE) with the extent of surface coverage (θ) (Foad, 1999). From Table 1, values of $\theta \approx 0.65$ (with 2000 ppm) and $\theta \approx 0.75$ (with 2000 ppm + 1 mM KI) confirm that the inhibitor molecules could effectively adsorb on the active sites of the stainless steel surface, and that the iodide ions further promote this adsorption and spreading into a highly protective layer (Onyeachu and Solomon, 2020). In acid-type environments, several authors have also reported improved efficiency of corrosion inhibitors courtesy of synergistic action of iodide ions (Onyeachu et al., 2021; Umoren et al., 2010). On one hand, the synergism could be competitive, whereby, iodide ions and corrosion inhibitor molecules jostle for adsorption on positively-charged anodic sites on the metal surface. Since the corroding alloy surface has an abundance of these adsorption sites, such jostling could translate into quicker occupation and surface coverage by both 1-benzylimidazole and iodide ions. On the other hand, the synergism could be cooperative, whereby the adsorption of one species does not interfere with the adsorption of the other but promotes the inhibitor adsorption. This could occur when preliminarily adsorbed iodide ions induce a net negative charge and form intermediate bridges that promote 1-benzylimidazole-metal interaction. The synergism parameter ($S_\theta = \frac{1-\theta_{1+2}}{1-\theta_{1+2}}$) (Aramaki and Hackerman, 1969) can elucidate whether competitive or cooperative synergism is dominant, whereby, $\theta_{1+2} = \theta_1 + \theta_2 - (\theta_1\theta_2)$, θ_1 = degree of surface coverage of 1-benzylimidazole, θ_2 = degree of surface coverage of iodide

Table 1 Weight loss and corrosion rate values measured for 316 L stainless steel after 6 and 72 h immersion in 1 M HCl without and with different 1-benzylimidazole concentrations and with 1 mM KI addition at 60 °C.

Inhibitor Conc. (ppm)	Weight loss \pm S.D. (g)	Corrosion Rate \pm S.D. (mm/yr)	% IE (%)
6 h			
Blank	0.160 ± 0.014	12.87 ± 1.59	–
500	0.105 ± 0.007	8.44 ± 0.79	34.26 ± 1.94
1000	0.085 ± 0.007	6.84 ± 0.80	46.86 ± 0.39
1500	0.070 ± 0.000	5.63 ± 0.00	55.91 ± 5.46
2000	0.056 ± 0.007	4.90 ± 1.36	65.12 ± 1.87
1 mM KI	0.064 ± 0.004	5.15 ± 0.46	59.91 ± 1.42
2000 ppm + 1 mM KI	0.024 ± 0.004	1.93 ± 0.46	85.03 ± 0.44
72 h			
Blank	0.230 ± 0.000	15.41 ± 0.00	–
2000	0.099 ± 0.004	6.63 ± 0.46	56.98 ± 1.42
1 mM KI	0.101 ± 0.007	6.77 ± 1.79	56.07 ± 1.94
2000 ppm + 1 mM KI	0.060 ± 0.002	4.55 ± 0.21	73.91 ± 0.39

ions, and θ'_{1+2} = the degree of surface coverage of 1-benzylimidazole + iodide ions. A competitive mechanism is dominant if $S_\theta < 1$, while $S_\theta > 1$ indicates the cooperative mechanism. As calculated from the weight loss results, the value of $S_\theta = 0.9339$ is less than unity and indicates a competitive synergism between 1-benzylimidazole and the iodide ions. Competitive synergism has also been reported between iodide ions and some cationic corrosion inhibitors in acid solutions (Mouheddin et al., 2019; Mouheddin et al., 2018).

3.2. Adsorption isotherm

Corrosion inhibitor–metal substrate interaction usually involves reversible adsorption–desorption processes that could proceed to a chemical equilibrium. Understanding the mechanism of inhibitor adsorption and the nature of the equilibrium established requires the use of adsorption isotherms. In the present work, the interaction between corrosion inhibitor and the stainless steel substrate was tested with the Langmuir, Temkin and Freundlich models using data obtained from the weight loss experiment. According to Eq. (6) (Akinbulumo et al., 2020), the Langmuir isotherm assumes that a linear relationship exists between the extent of metal surface coverage (θ) by inhibitor and the inhibitor concentration (C). It also predicts that the corrosion inhibitor only adsorbs as a monolayer with negligible inhibitor–inhibitor interaction during adsorption (Akinbulumo et al., 2020). The adsorption equilibrium constant (K_{ads}) can be deduced from the inverse of the intercept at $C = 0$ ppm. The Freundlich isotherm relates the logarithms of surface coverage and inhibitor concentration using the Eq. (7) (Akinbulumo et al., 2020). From the slope of Freundlich plot ($\frac{1}{n}$), the extent of metal surface heterogeneity, and the intensity of inhibitor adsorption, can be predicted. Inhibitor adsorption is highly feasible when $0 < \frac{1}{n} < 1$ but moderate or difficult, respectively, when $\frac{1}{n} = 1$ or $\frac{1}{n} > 1$ (Chaudhary and Tak, 2022). Lastly, the Temkin isotherm assumes that a multi-layer interaction exists between the inhibitor molecules and the metal surface (Chaudhary and Tak, 2022). According to Eq. (8), a plot of θ vs. $\ln C$ should yield a straight line (with $R^2 \approx 1$) whose slope can be extrapolated to describe the lateral interaction between inhibitor and metal surface (α). Compared with the Langmuir and Temkin models in Fig. 2(a) and (c), respectively, the Freundlich model in Fig. 2(b) provides the best description for the inhibitor–metal interaction. The best agreement exists between experimental points and the fitting line for which $R^2 = 0.9995$. It indicates that the corrosion inhibitor interacts with a strongly heterogeneous stainless steel surface, caused by the high temperature which promotes surface attack by the acid solution. However, the value of $\frac{1}{n} = 0.4$, extrapolated from the slope of the Freundlich plot, confirms that the inhibitor adsorption is highly feasible under the testing condition. Therefore, abundant active sites are exposed on the stainless steel surface during the acid corrosion at 60 °C, and these active sites accommodate more inhibitor, which explains why the inhibition efficiency increases with concentration.

$$\frac{C}{\theta} = \frac{1}{K_{ads}} + C \quad (6)$$

$$\log \theta = \log K_{ads} + \frac{1}{n} \log C \quad (7)$$

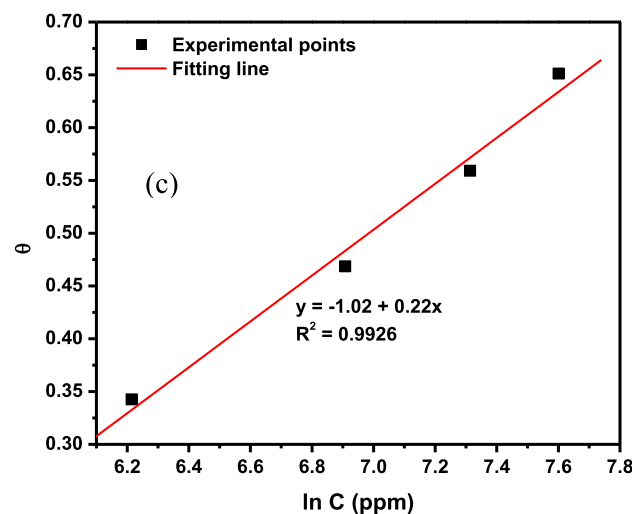
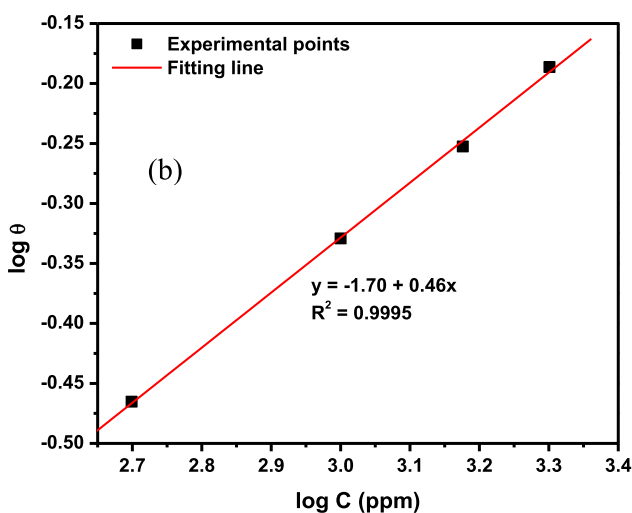
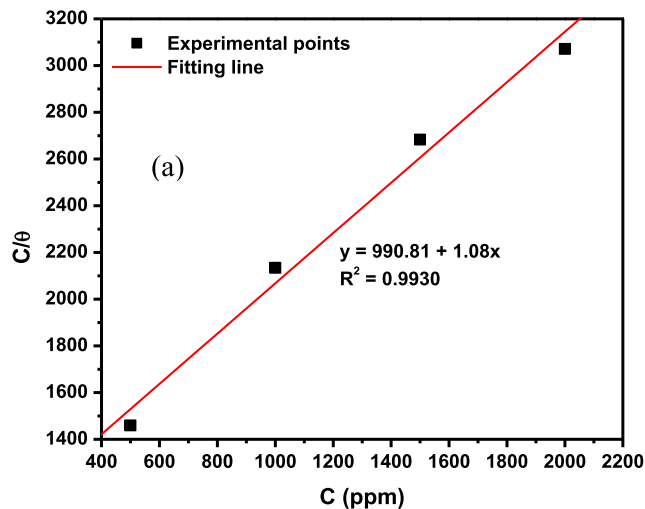


Fig. 2 (a) Langmuir (b) Freundlich and (c) Temkin and isotherm plots for the adsorption of 1-benzylimidazole on SS316L stainless steel during corrosion in 1 M HCl at 60 °C.

$$\theta = -\frac{1}{2\alpha} \ln C - \frac{1}{2\alpha} K_{ads} \quad (8)$$

3.3. Electrochemical results

3.3.1. Electrochemical impedance spectroscopy (EIS) results

After 1800 s of free immersion in the acid solution without and with 500 and 2000 ppm of 1-benzylimidazole, 1 mM KI, and 2000 ppm + 1 mM KI, the stainless steel could attain a stable open circuit potential (OCP), as revealed in Fig. 3. At the OCP, Fig. 4 presents the potentiostatic EIS results. In Fig. 4 (a), the Nyquist plots are similar in shape but differ in sizes. The addition of 1-benzylimidazole increases the Nyquist arc only minimally at 500 ppm dosage, but quite significantly at 2000 ppm. The observed enlargement of the Nyquist arcs testify to increased corrosion resistance impacted on the stainless steel by 1-benzylimidazole. Furthermore, the Fig. 4(a) reveals that, although the addition of 1 mM KI impacted greater corrosion resistance than the minimum inhibitor concentration (500 ppm), the impact of the inorganic molecule was lower than that delivered by the maximum inhibitor concentration (2000 ppm). Remarkably, too, the combination of 2000 ppm 1-benzylimidazole with 1 mM KI exhibited the largest Nyquist arc in Fig. 4(a). The Nyquist results are further confirmed by the absolute impedance plot in Fig. 4(b), whereby the value of impedance at low frequency is highest for the 1-benzylimidazole + KI system and least for the blank solution. Clearer interpretation of the corrosion inhibition mechanism is provided by the phase angle plots in Fig. 4(c). The plots reveal both high frequency and low frequency peaks for all the corrosion conditions. Generally, the stainless steel exhibits higher phase angle peaks in the presence of corrosion inhibitor, becoming most significant with the 1-benzylimidazole + KI corrosion inhibitor system. The peak at high frequency depicts the charge-transfer phenomenon occurring at a passive layer-solution interface, whereas the low frequency peak signifies the phenomena at the passive layer-substrate interface. Rationally, this passive layer consists of the nucleating oxides/hydroxides of Fe and Cr (in the absence of inhibitor) as well as the adsorbed inhibitor molecules (in the presence of inhibitor). The two-time constants equivalent circuit in Fig. 4(d) was

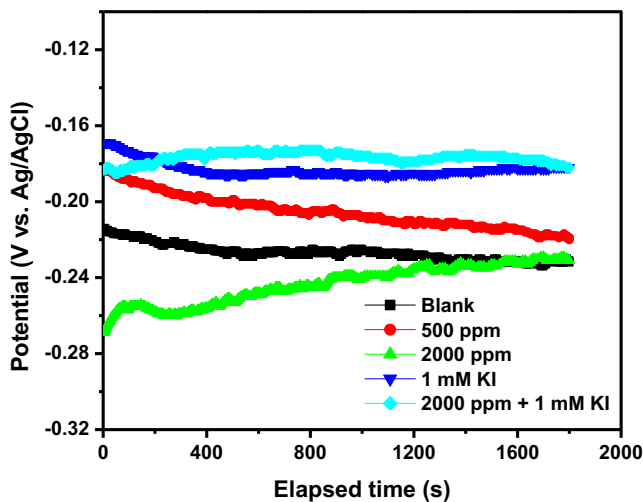


Fig. 3 Variation of open circuit potential (OCP) with time for SS316L stainless steel during corrosion in 1 M HCl at 60 °C without and with 1-benzylimidazole 500 ppm, 2000 ppm, 1 mM KI and 2000 ppm + 1 mM KI.

adopted to provide electrical description of the corrosion and inhibition mechanism. The confidence in choosing the two-time constants is further boosted by the good agreement between the experimental plots and fitting lines (Fig. 4e) and the low goodness-of-fit values in Table 2. The first-time constant describes the passive layer-solution interface using the resistance of layer to porosity (R_f) and the layer capacitance (CPE_f). The second time constant uses the charge transfer resistance (R_{ct}) and double layer capacitance (CPE_{dl}) to describe the electric double layer existing at the passive layer-substrate interface. The constant phase element (CPE), rather than pure capacitor, is adopted in Fig. 4(d), in order to account for surface roughness of the corroding alloy. The CPE consists of an admittance element (Y) and a roughness parameter (n : $-1 \leq n \leq 1$) (Hsu and Mansfeld, 2001). In the double layer, however, the double layer capacitance (C_{dl}) provides better accuracy than the admittance (Y_{dl}). The C_{dl} is calculated from Y_{dl} based on Eq. (9); whereby f_{max} is the frequency (Hz) which corresponds to the maximum impedance of the imaginary component in the Nyquist plot (Shoosmith et al., 1980). The extrapolated electrical elements have been presented in Table 1.

$$C_{dl} = Y_{dl}(2\pi f_{max})^{n-1} \quad (9)$$

At pH 1 and 3, Deen et al. (Deen et al., 2020) reported that Fe^{3+} and Cr^{3+} transport at stainless steel-solution interface controls the rate of corrosion and stability of passive film formed on uninhibited 316 L stainless steel. On the other hand, Tang et al. (Tang et al., 2019) established that the Cl^- ions in HCl can antagonize the stability of passive films formed on stainless steel by dissolving them as soluble chlorides and initiating severe localized corrosion attack. These factors would expose more alloy surface to the corrosion attack. In the presence of 1-benzylimidazole, however, the rate of Fe^{3+} and Cr^{3+} release/transport is suppressed because the reactive centers (nitrogen atom and C = C bond) engage in electron donation and acceptance with the d-orbitals in Fe and Cr atoms. More so, as a protonated species in acid solution (Solomon et al., 2020); 1-benzylimidazole could also engage in an indirect adsorption through electrostatic attraction to anionic species pre-adsorbed on the alloy surface due to attraction to Fe^{3+} and Cr^{3+} . For this latter case, the Cl^- and I^- ions provide the template for such inhibitor adsorption (Umoren and Solomon, 2014; Cardona et al., 2014; Onyeachu et al., 2019). This enhanced inhibitor adsorption on the stainless steel surface shields the alloy from the solution, and the deteriorating impact of Cl^- ions are minimized (since a fraction of the ions likely boost inhibitor adsorption). Consequently, a promoted Fe/Cr-oxide/hydroxide formation proceeds within the double layer in the presence of 1-benzylimidazole which becomes even enhanced with KI addition. Thus, the single inhibitor, at 2000 ppm, exhibits inhibition efficiency approximately 67 %, which is boosted to 78 % due to addition of 1 mM KI.

3.3.2. Cyclic potentiodynamic polarization (CPDP)

The cyclic potentiodynamic polarization (CPDP) plots for SS 316L stainless steel in 1 M HCl solution without and with 500 and 2000 ppm of 1-benzylimidazole, 1 mM KI, and 2000 ppm + 1 mM KI are presented in Fig. 5(a)–(e), respectively. The polarization parameters extrapolated from the plots, such as corrosion potential (E_{corr}), corrosion current

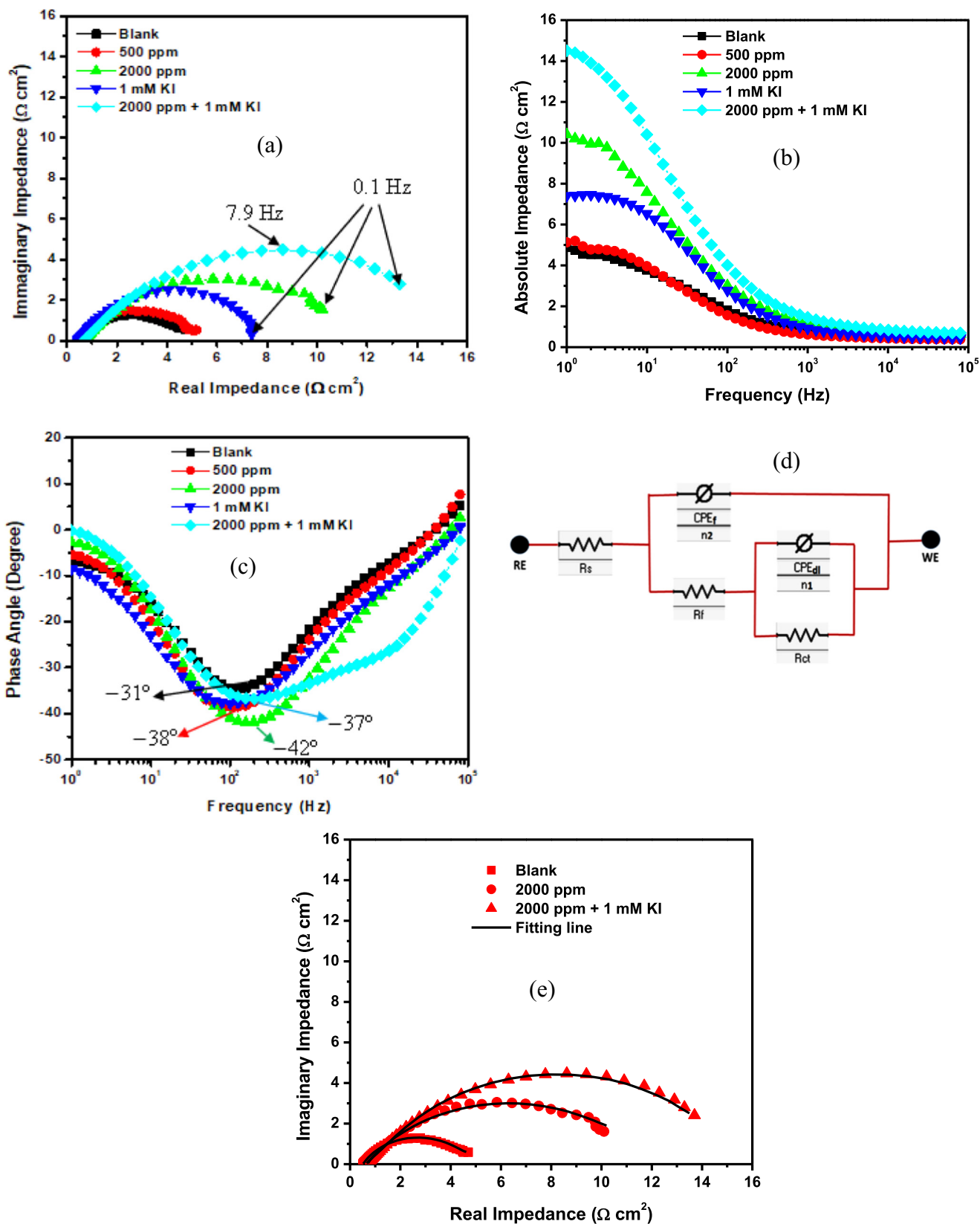


Fig. 4 EIS plots (a) Nyquist (b) absolute impedance (c) phase angle and (d) equivalent circuit for SS316L stainless steel during corrosion in 1 M HCl at 60 °C without and with 1-benzylimidazole 500 ppm, 2000 ppm, 1 mM KI and 2000 ppm + 1 mM KI.

Table 2 EIS parameters derived for SS316L stainless steel during corrosion in 1 M HCl at 60 °C without and with 1-benzylimidazole 500 ppm, 2000 ppm, 1 mM KI and 2000 ppm + 1 mM KI.

Conc. (ppm)	$R_s (\Omega \text{ cm}^2)$	CPE _{dl}			CPE _r			Goodness of Fit ($\times 10^{-3}$)	%IE
		$Y_{dl} (\text{mFcm}^{-2} \text{ s}^{-1})$	n_{dl}	$R_{ct} (\Omega \text{ cm}^2)$	$Y_r (\mu\text{Fcm}^{-2} \text{ s}^{-1})$	n_r	$R_r (\Omega \text{ cm}^2)$		
0	0.51 ± 0.005	6.71 ± 0.001	0.69 ± 0.009	4.34 ± 0.01	8.35 ± 0.10	0.81 ± 0.10	0.40 ± 0.13	0.89	–
500	0.59 ± 0.004	7.19 ± 0.004	0.70 ± 0.007	5.02 ± 0.08	1.13 ± 0.19	0.89 ± 0.020	2.41 ± 0.63	2.13	36.14 ± 0.14
2000	0.63 ± 0.008	6.01 ± 0.003	0.72 ± 0.010	11.29 ± 0.23	5.01 ± 0.07	0.90 ± 0.190	5.24 ± 0.21	0.95	71.27 ± 0.10
KI	0.56 ± 0.008	2.16 ± 0.008	0.70 ± 0.007	6.46 ± 0.09	3.24 ± 0.01	0.71 ± 0.006	3.07 ± 0.16	1.45	50.26 ± 0.01
2000 + KI	0.70 ± 0.002	2.76 ± 0.006	0.79 ± 0.001	15.71 ± 0.01	5.75 ± 0.06	0.90 ± 0.009	6.10 ± 0.01	0.58	78.26 ± 0.06

density (i_{corr}), passivation (E_{pass}), re-passivation potential (E_{rp}) and pitting potential (E_{pit}) are presented in Table 3. The forward potential scan shows regions of active corrosion and passivation, while the reverse scan shows regions of pitting and re-passivation. The E_{corr} and i_{corr} were derived by extrapolating the cathode–anode potential transition in the active region around ± 10 mV. The addition of 1-benzylimidazole is observed to shift the E_{corr} more anodically from -247.09 mV in the blank solution to -232.55 mV in the presence of 2000 ppm inhibitor. The inhibitor addition also attenuates both cathodic and anodic currents. The observed extent of potential shift, however, is not enough to qualify 1-benzylimidazole as a purely anodic corrosion inhibitor (Onyeachu et al., 2021). Rather, the inhibitor is a mixed-type inhibitor with slightly more anodic impact. 1-benzylimidazole impacted a similar anodic effect on carbon steel corroding in acidic $\text{H}_2\text{S} + \text{CO}_2$ -saturated solution (Onyeachu et al., 2021). This anodic effect suggests that 1-benzylimidazole is more inclined to mitigate the stainless steel active corrosion in 1 M HCl at 60 °C by interfering more with the $\text{Fe} \rightarrow \text{Fe}^{2+}$ and $\text{Cr} \rightarrow \text{Cr}^{3+}$ oxidation processes, rather than $\text{H}^+ \rightarrow \text{H}_{2(g)}$ reaction. By donating free electrons from the nitrogen and C=C active centres into the unfilled d-orbitals of Fe and Cr, the inhibitor suppresses oxidative dissolution of the alloy. The suppression of the anodic processes shunts the electron flow that sustains cathodic reduction of H^+ . This explains why both cathodic and anodic currents are lowered upon 1-benzylimidazole addition. At 2000 ppm dosage, the corrosion inhibitor suppresses the stainless steel corrosion with 70.76 % efficiency. The addition of KI, alone ($E_{corr} = -195.64$ mV) and in combination with 1-benzylimidazole ($E_{corr} = -181.67$ mV), exerts further anodic shift on the corrosion potential and further lowers corrosion current density. This Γ^- effect elevates the 1-benzylimidazole inhibition efficiency to 81.36 %. Given the competitive synergism existing between Γ^- and 1-benzylimidazole ($S_0 = 0.85$) and the changes in E_{corr} in the presence of KI, we are compelled to posit that the competitive adsorption of Γ^- could instigate 1-benzylimidazole to interact more with Cl^- ions to boost the anodic inhibition mechanism. This mechanism significantly diminishes $\text{Fe} \rightarrow \text{Fe}^{2+}$ and $\text{Cr} \rightarrow \text{Cr}^{3+}$ oxidation.

The mechanism of passivation is the same whether the stainless steel corrodes in the acid without and with 1-benzylimidazole and 1-benzylimidazole + KI. The inhibitor systems appear to have insignificant effect on the passivation potential and current. The inhibitor addition, however, lowers the pitting potential (E_{pit}) from 174.88 mV in blank to 133.24 mV with 2000 ppm 1-benzylimidazole and 124.54 mV with 1-benzylimidazole + KI, as Table 3 shows. This result strongly suggests that the 1-benzylimidazole and 1-benzylimidazole + KI corrosion inhibitor systems mostly decrease the corrosion rate of the stainless steel during its active corrosion. During passivation, however, the growing oxide/hydroxide scales seem to depreciate the adsorption of the inhibitor species because they block the outward diffusion of Fe^{2+} and Cr^{3+} ions from the substrate to the reaction front where interaction with both 1-benzylimidazole and Γ^- usually occurs. This would weaken the adsorption strength between substrate and inhibitor species, thereby, encouraging detachment of the adsorbed inhibitor layer. This detachment is liable to open new active sites which trigger localized pitting corrosion on the alloy surface. Howbeit, the reverse CPDP scan shows negative hystere-

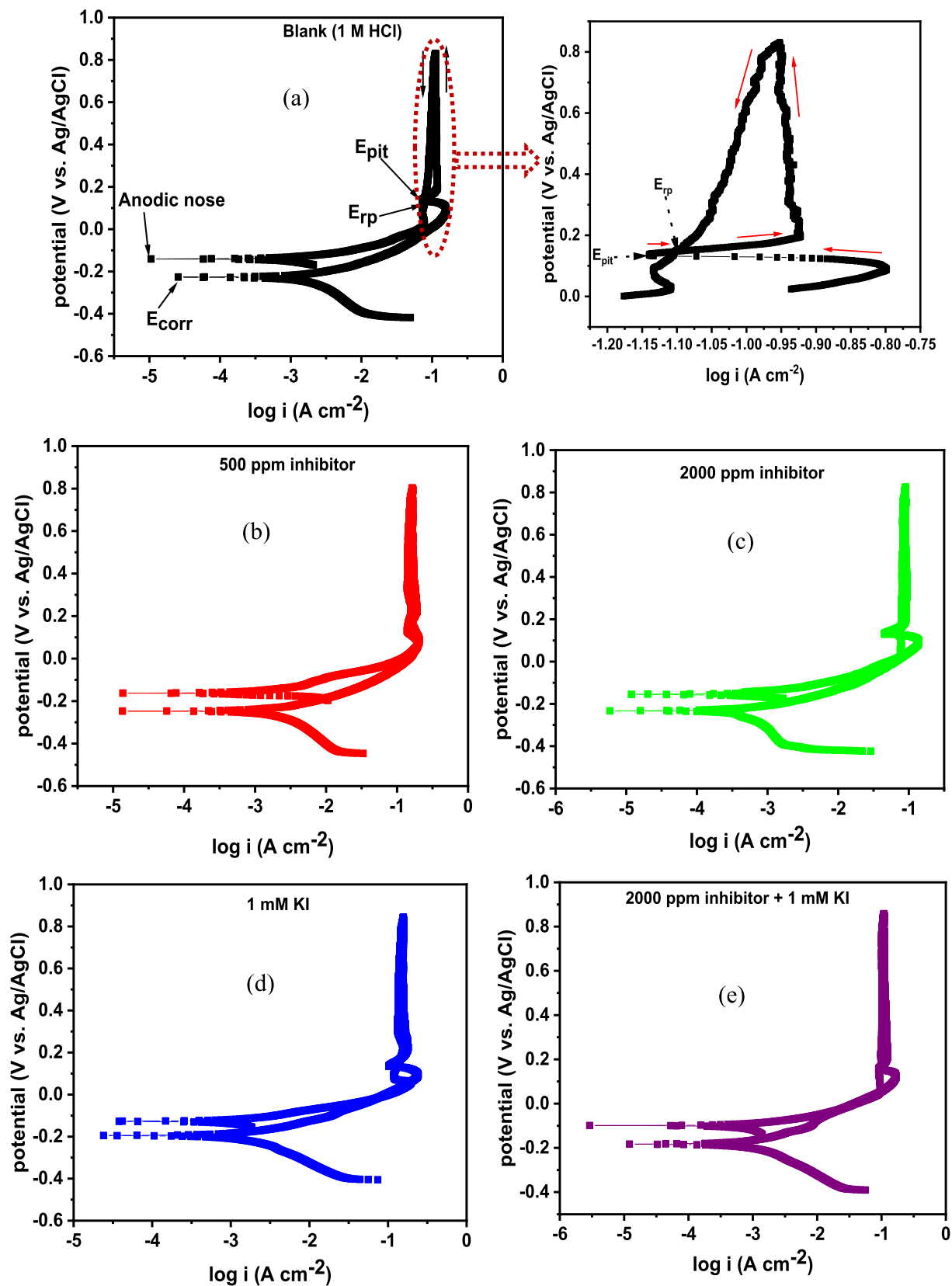


Fig. 5 CPDP plots obtained for SS316L stainless steel during corrosion in 1 M HCl at 60 °C without and with 1-benzylimidazole 500 ppm, 2000 ppm, 1 mM KI and 2000 ppm + 1 mM KI.

Table 3 CPDP parameters derived for SS316L stainless steel during corrosion in 1 M HCl at 60 °C without and with 1-benzylimidazole 500 ppm, 2000 ppm, 1 mM KI and 2000 ppm + 1 mM KI.

System	$-E_{\text{corr}}$ (mV _{Ag/AgCl})	i_{corr} (mA cm ⁻²)	E_{pit} (mV _{Ag/AgCl})	E_{rp} (mV _{Ag/AgCl})	$E_{\text{pit}} - E_{\text{rp}}$ (mV _{Ag/AgCl})	- Anodic nose (mV _{Ag/AgCl})	Anodic nose - E_{corr} (mV _{Ag/AgCl})	%IE
Blank	247.09	2.36	174.88	120.98	53.90	162.57	-84.52	-
500 ppm	227.43	1.66	141.95	87.93	54.02	140.66	-86.77	29.73
2000 ppm	232.55	0.69	133.24	22.51	110.73	155.12	-77.43	70.76
1 mM KI	195.64	1.28	134.96	65.97	68.99	127.43	-68.21	45.76
2000 ppm + 1 mM KI	181.67	0.44	124.54	21.65	102.89	99.10	-82.57	81.36

sis loops for all tested conditions, whereby lower current densities are acquired compared with the forward scan (Tait, 2018; Esmailzadeh et al., 2018). This implies plausibility of the alloy to self-heal and repair any damage to its passive layer, both without and with corrosion inhibitor (Tait, 2018; Esmailzadeh et al., 2018). Nevertheless, larger size of hysteresis loop is also indicative of greater damage to a passive film and more difficulty in self-healing (Esmailzadeh et al., 2018). When Fig. 5(a) is compared with other results in Fig. 5, it can be affirmed that the inhibited system can achieve self-healing more readily, especially the 1-benzylimidazole + KI, than the alloy in the blank solution. This self-healing may be achieved when the inhibitor species penetrate into the localized pits (where Fe²⁺ and Cr³⁺ are rapidly released from substrate), adsorb therein and seal the pits/encourage protective Fe/Cr-oxide/hydroxide re-growth. The ease of re-passivation and the persistence of the re-passivated layer can be assessed by the nobility of re-passivation potential (E_{rp}) and the anodic nose, relative to the corrosion potential (E_{corr}) (Tait, 2018; Esmailzadeh et al., 2018). The nobler the E_{rp} and anodic nose values, relative to the E_{corr} , the easier is the re-passivation and more persistent is the re-passivated layer (Moravcik et al., 2021; Loto and Solomon, 2021). The values of E_{rp} and anodic nose are nobler with respect to their respective E_{corr} values, in the inhibited solutions, compared with the blank solution. These results confirm that 1-benzylimidazole is an effective corrosion inhibitor for 316L stainless steel in 1 M HCl at 60 °C, and that the addition of 1 M KI provides further boost to this effectiveness.

3.3.3. Cyclic voltammetry (CV)

The mechanism of corrosion inhibition by 1-benzylimidazole and 1-benzylimidazole + KI formulation was further elucidated using the cyclic voltammetry. For all the tested conditions, the voltammograms in Fig. 6 reveal two anodic and cathodic peaks, each, in the forward and reverse potential scan. Both peaks in the forward scan occur within the potential range where the alloy exhibits passivation, as the CPDP results previously showed. These peaks are the anodic currents emanating from the rate of oxidation of Fe and Cr into oxides and hydroxides during the corrosion (Ait Albrimi et al., 2011; Mulimbayan and Mena, 2016; Knapp and Wren, 2012). Higher current values in the voltammograms, therefore, depict higher rate of corrosion and greater susceptibility to localized corrosion like pitting. Lower current values depict slower rate of oxidation leading to slower rate (and more stable) rate of growth of the passive layer. The voltammograms confirm that the addition of 1-benzylimidazole in the

1 M HCl solution at 60 °C clearly diminished the current peaks, and this effect is more established when 1 mM KI is added. This confirms that 1-benzylimidazole and I⁻ adsorption shunts electron transfer between anodic surface and cathodic sites on the corroding alloy. This shunting also explains why the cathodic peaks in the reverse scan exhibit the least current values in the 1-benzylimidazole + KI system. These peaks must be signals from several reduction reactions involving H⁺ → H₂, Fe²⁺ → Fe and Cr³⁺ → Cr (Ait Albrimi et al., 2011; Mulimbayan and Mena, 2016; Knapp and Wren, 2012). Nevertheless, the voltammetry peaks for both uninhibited and inhibited stainless steel appear around the same potentials during both forward and backward scans. This confirms the CPDP result which showed that the stainless steel passivation mechanism is not altered, but strongly enhanced, by the presence of both 1-benzylimidazole and I⁻ in the acid solution.

3.4. Effect of time

The weight loss and electrochemical results confirm that 1-benzylimidazole is an efficient inhibitor against the corrosion of SS 316L stainless steel in 1 M HCl solution at 60 °C, and its combination with KI is even more formidable for protecting

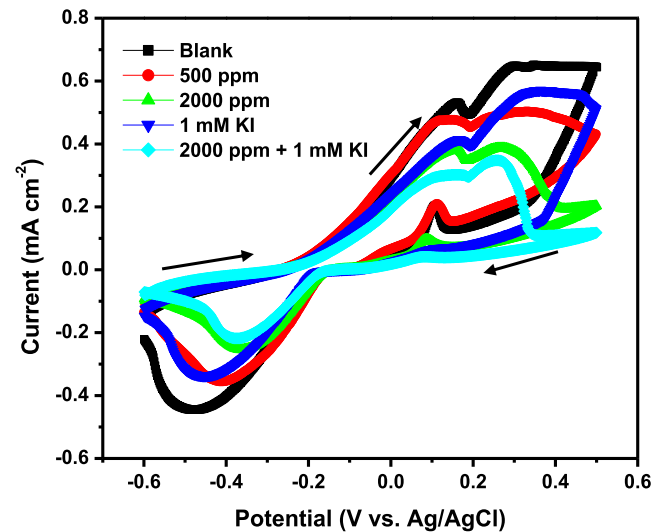


Fig. 6 Cyclic voltammetry results obtained for SS316L stainless steel during corrosion in 1 M HCl at 60 °C without and with 1-benzylimidazole 500 ppm, 2000 ppm, 1 mM KI and 2000 ppm + 1 mM KI.

the alloy. However, these are only short-term performances. Depending on the extent of scaling on heat exchangers, acid cleaning operations could involve long term contact (up to 72 h (Onyeachu and Solomon, 2020) between the acid solution and the stainless steel material. For this reason, the performances of 1-benzylimidazole, KI and 1-benzylimidazole + KI were investigated after 72 h immersion, and the results obtained are presented in Table 1. Compared with the results obtained after 6 h immersion, the stainless steel generally experiences an increase in both weight loss and corrosion rate, after 72 h. The inhibition efficiency for each corrosion inhibitor system also decreased. Since the uninhibited and inhibited alloy could passivate in the short run, as confirmed by the electrochemical measurements, this increase in weight loss and corrosion rate after 72 h implies that the passive layer becomes deteriorated and inhibitor desorption sets in.

Over the 72 h, more corrosion-inducing species like H^+ and Cl^- ions accumulate at the alloy-solution interface. They become enabled to compete more strongly (for adsorption) with the inhibitor species. For instance, the Cl^- ions are well-known to form soluble metal complexes which induce localized degradation of the passive layer and detachment of adsorbed corrosion inhibitor species (Onyeachu et al., 2020). The passive layer consumption increases its porosity and promotes outward diffusion of Fe^{2+} and Cr^{3+} ions to leave the underlying alloy substrate and migrate to the passive layer-solution interface for the replenishment of lost Fe/Cr-oxides/hydroxides and/or interaction with corrosion inhibitor species. When the changes in inhibition efficiency between 6 h and 72 h are considered, it appears that, during the longer immersion time, the greater attack by H^+ and Cl^- ions affects the performance of 1-benzylimidazole (from $65.12\% \pm 1.87$ to $56.98\% \pm 1.42$) more than it affects the performance of iodide ions (from $59.91\% \pm 1.42$ to $56.07\% \pm 1.94$). This observation is remarkable because it buttresses our previous position that the competitive adsorption of iodide ions at the anode could compel 1-benzylimidazole to interact more synergistically with Cl^- ions. Thus, the stronger bond between Fe/Cr and iodide ions makes desorption more difficult, whereas the accumulated Cl^- ions at

the alloy surface induces passive layer deterioration more than synergism with 1-benzylimidazole. This iodide effect is also the reason that, although the efficiency of the 1-benzylimidazole + KI system depreciated from $85.03\% \pm 0.44$ (6 h) to $73.91\% \pm 0.39$ (72 h), it still provided the best protection compared with the individual inhibitors. This observation, therefore, underscores the importance of iodide ions in the formulation of organic-based acid cleaning corrosion inhibitors. In Table 4, a comparison is made between the efficiency of some reported corrosion inhibitors and the efficiency of our 1-benzylimidazole + KI system for stainless steel corrosion inhibition in acid solutions at elevated temperatures.

3.5. SEM characterization

The Fig. 7 represents the surface morphologies exhibited by the 316L stainless steel alloy after 6 h immersion in 1 M HCl solution at 60 °C without and with 2000 ppm 1-benzylimidazole + 1 mM KI. In Fig. 7(a), a highly degraded surface characterizes the stainless steel surface after corrosion in the absence of the 1-benzylimidazole + 1 mM KI inhibitor formulation. Patches of smooth surfaces are heavily surrounded by large pits propagating into large and deep holes that expose the interior of the alloy. At some other portions, the holes are relatively shallower, but definitely represent some layer detachment from the alloy surface. The smooth patches are attributed to the areas where passivation has been sustained on the alloy surface during the immersion duration. The shallower holes represent regions where passivation extends deeper into the alloy surface and is, somewhat, sustained even after some delamination. On the other hand, the regions showing large and deep holes indicate regions of greater susceptibility to localized chloride attack which converts protective oxides/hydroxides into soluble chlorides. When 1-benzylimidazole + 1 mM KI is added to the acid solution, Fig. 7(b) shows that the pits on the alloy become smaller in size and shallower in depth. A layer is seen to cover the alloy surface and shield the tiny pits and alloy surface from the corrosion environment. This confirms that the corrosion inhibitor system adsorbs and

Table 4 Comparative analysis of the performance of 1-benzylimidazole + KI and some reported corrosion inhibitors for stainless steel corrosion inhibition in acid solutions at elevated temperatures.

S/N	Inhibitor system	Corrosion system	Inhibitor Dose	Temp. (°C)	Maximum inhibition efficiency (%)	Ref
1	Rhodamine azosulfa drugs	304SS in 1 M HCl	1.0×10^{-3} M	60 °C	62.86	(Abdallah, 2002)
2	Adenine	304SS in 1.1 M HCl	0.5×10^{-3} M	60 °C	60.0	(Scendo and Trela, 2013)
3	Garlic extract	304SS in 1.1 M HCl	10 cc/L	70 °C	87.9	(Asfia et al., 2020)
4	Amino cadalene	321SS in 1 M H ₂ SO ₄	1.0×10^{-3} M	50 °C	16.15	(Koumya et al., 2020)
5	Barley agro-industrial waste	AISI 304 in H ₂ SO ₄	1 g/L	52 °C	53.40	(Matos et al., 2018)
6	Egg shell powder	321SS in 1 M H ₂ SO ₄	10 g/L	35 °C	91.16	(Sanni et al., 2019)
7	Egg shell powder	201SS in 1 M HCl	21×10^6 M	45 °C	63.90	(Fouda et al., 2018)
8	5-Azidomethyl-8-Hydroxyquinoline	AISI 321 in 5.5 M H ₃ PO ₄	2.2×10^{-2} M	60 °C	49.00	(Mazkour et al., 2021)
9	1-benzylimidazole	SS 316 L in 1 M HCl	2000 ppm 2000 ppm + 1 mM KI	60 °C 60 °C	71.27 85.03	This Work

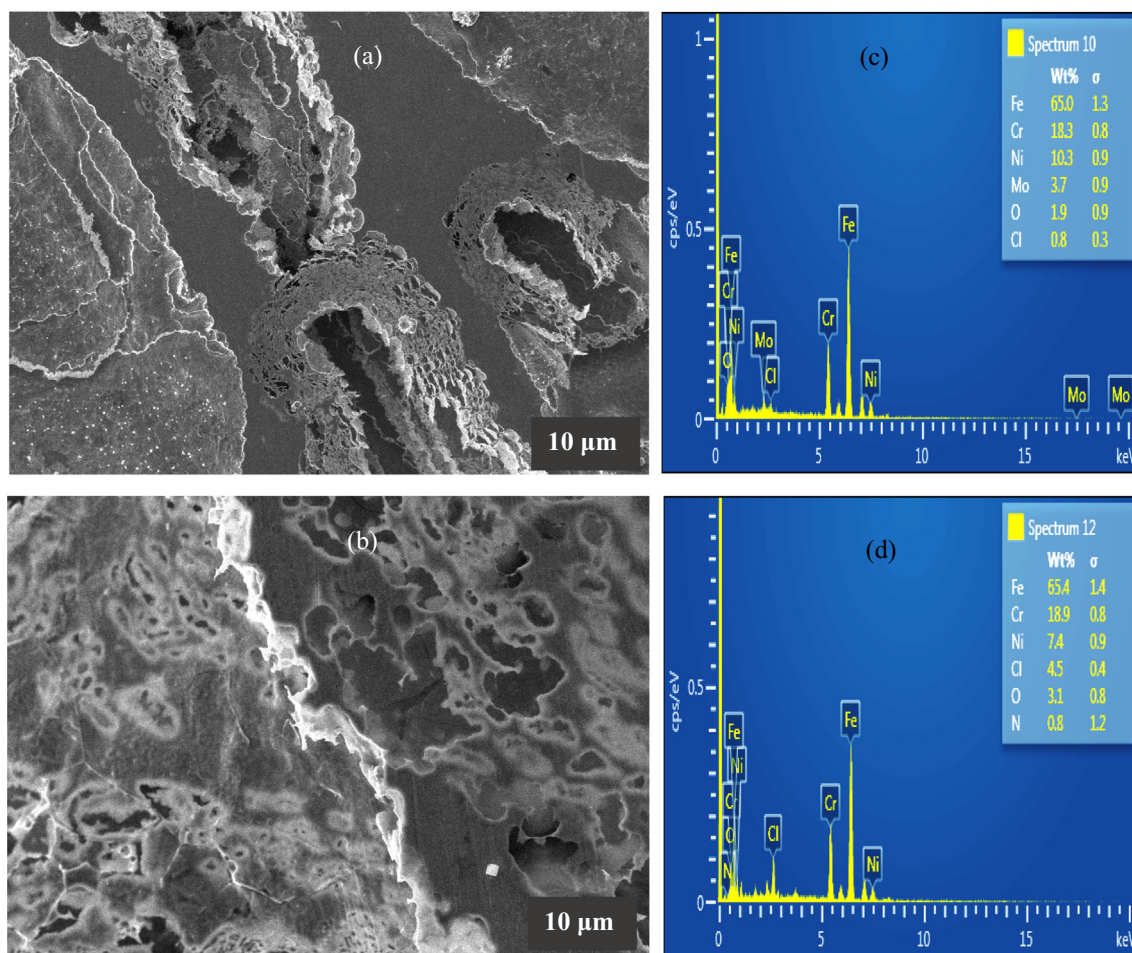


Fig. 7 SEM–EDX surface images ($\times 1000$) for SS316L stainless steel after corrosion in 1 M HCl at 60 °C (a,c) without and (b,d) with 2000 ppm 1-benzylimidazole + 1 mM KI.

enhances the re-passivation of the stainless steel during the acid corrosion, in accordance with the CPDP finding. The associated EDAX results in Fig. 7(c) and (d) provides important information which could support the proposed adsorption mechanism of 1-benzylimidazole. The lower composition of Cl detected on the alloy surface in the absence of inhibitor strongly supports that the attack on the passive layer causes substantial dissolution of the formed chlorides (i.e. loss from the surface). On the other hand, the chloride ions facilitate inhibitor adsorption since the alloy displays higher Cl composition (which are reasoned to be domiciled on the surface). The 1-benzylimidazole adsorption is further confirmed by the detection of N in the EDAX result of Fig. 7(d).

3.6. Proposed mechanism

Preliminary works have shown that 1-benzylimidazole exists, most likely, as a cationic species in an acid solution (Onyeachu et al., 2021). On this basis, the following mechanism can be suggested to explain the corrosion inhibition characteristics of 1-benzylimidazole and the influence of iodide ions on 1-benzylimidazole performance. As a cationic species, 1-benzylimidazole can adsorb on both cathodic and anodic

sites on the alloy surface, but it is more inclined to anodic adsorption through electronic interaction with the incompletely-filled d-orbitals of Fe^{2+} and Cr^{3+} . This anodic interaction is enhanced by Cl^- ions pre-adsorbed on the stainless steel surface. Once effectively adsorbed on the stainless steel surface, the inhibitor layer extends its hydrophobic phenyl group into the solution phase which then repels incoming corrosion-inducing species, especially, the Cl^- ions. This encourages simultaneous inhibitor adsorption and passive layer formation and, eventually explains the remarkable corrosion inhibition efficiency recorded in the HCl solution containing 2000 ppm 1-benzylimidazole. When KI is added to the 1-benzylimidazole-containing acid solution, the negatively-charged iodide ions compete with the 1-benzylimidazole in order to interact electrostatically with the $\text{Fe}^{2+}/\text{Cr}^{3+}$ on the stainless steel surface. This competition, which is confirmed by a synergism parameter less than unity, constrains 1-benzylimidazole to interact with $\text{Fe}^{2+}/\text{Cr}^{3+}$ through pre-adsorbed Cl^- ions, as confirmed by the SEM-EDX characterization. In the short run, this competitive adsorption favours greater anodic site coverage, as confirmed by the E_{corr} values in the CPDP measurement. In the long run, however, the accumulation of more Cl^- ions at the stainless steel surface could

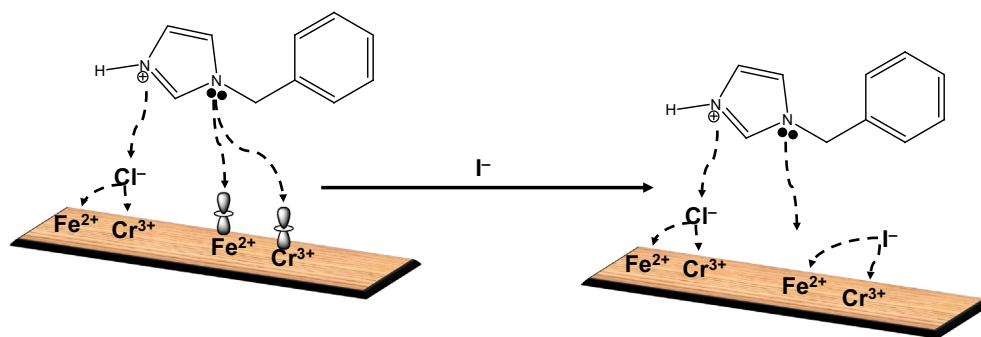


Fig. 8 Schematic representation of the inhibition mechanism of 1-benzylimidazole and synergistic influence of iodide ions.

induce passive layer deterioration through localized pitting corrosion, rather than facilitate a stronger 1-benzylimidazole- Cl^- ion- $\text{Fe}^{2+}/\text{Cr}^{3+}$ interaction. This proposed mechanism is elucidated in the schematic representation in Fig. 8.

4. Conclusion

In this work, we have investigated 1-benzylimidazole and its mixture with KI as a promising low-toxic corrosion inhibitor system to mitigate the corrosion of heat exchanger-type stainless steel alloy SS 316 L during acid cleaning in 1 M HCl solution at 60 °C. Weight loss measurements, after 6 h and 72 h immersion periods, enabled us to optimize 1-benzylimidazole concentration and analyse the effect of time on the performance of the 1-benzylimidazole + KI mixture. Electrochemical measurements with the optimum 1-benzylimidazole concentration enabled the determination of inhibitor mechanism, while SEM-EDX characterizations elucidated the impact of the 1-benzylimidazole + KI mixture to protect corrosion-induced surface degradation of the alloy. The conclusions drawn from the results obtained can be summarized. As a single inhibitor molecule, 1-benzylimidazole mitigates the stainless steel corrosion through adsorption, more preferentially, on the anodic sites to suppress oxidation reactions which lead to alloy dissolution in the acid. The adsorption, which follows the Freundlich isotherm, improves the characteristics of the stainless steel passive layer through synergistic interaction with pre-adsorbed Cl^- ions. At an optimum concentration of 2000 ppm, 1-benzylimidazole impacts an inhibition efficiency approximately 65 % after 6 h, but this efficiency decreases to approximately 57 % after 72 h. The addition of 1 mM KI to 2000 ppm 1-benzylimidazole significantly boosts the inhibitor efficiency to approximately 85 % and 74 % after 6 h and 72 h, respectively. Nevertheless, the iodide ions compete for anodic adsorption with 1-benzylimidazole, thus, encouraging the synergism between 1-benzylimidazole and Cl^- ions. The extent of this synergism, however, slightly depreciates in the long run (72 h) due to competition with localized pitting corrosion induced by the accumulated Cl^- ions at the stainless steel surface. Compared with literature reports, the 1-benzylimidazole + KI mixture is, certainly, a promising corrosion inhibitor to protect stainless steel heat exchangers during acid cleaning at high temperature.

Declaration of Competing Interest

The authors declare that they have no known competing financial interests or personal relationships that could have appeared to influence the work reported in this paper.

Acknowledgements

The authors acknowledged the contribution of Covenant University and Edo State University for providing some of the facilities used in this work.

References

- Obot, I.B., Meroufel, A., Onyechu, I.B., Alenazi, A., Sorour, A.A., 2019. Corrosion inhibitors for acid cleaning of desalination heat exchangers: Progress, challenges and future perspectives. *J. Mol. Liq.* 296.
- Malayeri, M.R., Jalalirad, M.R., 2014. Mitigation of crystallization scale in a single heated tube using projectiles of different sizes and hardness. *Heat Transf. Eng.* 35, 1418–1426.
- Onyechu, I.B., Solomon, M.M., 2020. Benzotriazole derivative as an effective corrosion inhibitor for low carbon steel in 1 M HCl and 1 M HCl + 3.5wt.% NaCl solutions. *J. Mol. Liq.* 313.
- Obot, I.B., Solomon, M.M., Onyechu, I.B., Umoren, S.A., Meroufel, A., Alenazi, A., Sorour, A.A., 2020. Development of a green corrosion inhibitor for use in acid cleaning of MSF desalination plant. *Desalination* 495.
- Yang, Q., Luo, J.L., 2000. The hydrogen-enhanced effects of chloride ions on the passivity of type 304 stainless steel. *Electrochim. Acta* 45, 3927–3937.
- Onyechu, I.B., Solomon, M.M., Umoren, S.A., Obot, I.B., Sorour, A. A., 2020. Corrosion inhibition effect of a benzimidazole derivative on heat exchange tubing materials during acid cleaning of multistage flash desalination plants. *Desalination* 479.
- Umoren, S.A., Solomon, M.M., Obot, I.B., Suleiman, R.K., 2021. Effect of Intensifier Additives on the Performance of Butanolic Extract of Date Palm Leaves against the Corrosion of API 5L X60 Carbon Steel in 15 wt.% HCl Solution. *Sustainability* 13, 5569.
- Iroha, N.B., Maduelosi, N.J., 2021. Corrosion Inhibitive Action and Adsorption Behaviour of Justicia Secunda Leaves Extract as an Eco-Friendly Inhibitor for Aluminium in Acidic Media. *Biointerface Res. Appl. Chem.* 11, 13019–13030.
- Solomon, M.M., Onyechu, I.B., Njoku, D.I., Nwanonyeni, S.C., Oguzie, E.E., 2021. Adsorption and corrosion inhibition characteristics of 2-(chloromethyl)benzimidazole for C1018 carbon steel in a typical sweet corrosion environment: Effect of chloride ion concentration and temperature. *Colloids Surf, A: Physicochem. Eng. Asp.* 610.
- Protocols on Methods for the Testing of Chemicals Used in the Offshore Oil Industry, Paris Commission (PARCOM), Paris, France, 2006.
- Shalini, K., Sharma, P.K., Kumar, N., 2010. Imidazole and its biological activities: A review. *Der Chemica Sinica* 1 (3), 36–47.
- Ranjith, R., 2016. The chemistry and biological significance of imidazole, benzimidazole, benzoxazole, tetrazole and quinazolinone nucleus. *Chem. Pharm. Res.* 8 (5), 505–526.
- Narasimhan, B., Sharma, D., Kumar, P., 2011. Biological importance of imidazole nucleus in the new millennium. *Med. Chem. Res.* 20 (8), 1119–1140.
- Balalaei, S., Arabanian, A., 2000. One-pot synthesis of tetrasubstituted imidazoles catalyzed by zeolite HY and silica gel under microwave irradiation. *Green Chem.* 2, 274–276.
- Keim, W.W., 2000. Ionic liquids—new solutions for transition metal catalysis. *Angew. Chem. Int. Ed. Eng.* 39, 3772–3789.

- Obot, I.B., Madhankumar, A., Umoren, S.A., Gasem, Z.M., 2015. Surface protection of mild steel using benzimidazole derivatives: experimental and theoretical approach. *J. Adhes. Sci. Technol.* 29, 2130–2152.
- Zhang, Z., Chen, S., Li, Y., Li, S., Wang, L., 2009. A study of the inhibition of iron corrosion by imidazole and its derivatives self-assembled films. *Corros. Sci.* 51, 291–300.
- Yan, T., Zhang, S., Feng, L., Qiang, Y., Lu, L., Fu, D., Wen, Y., Chen, J., Li, W., Tan, B., 2020. Investigation of imidazole derivatives as corrosion inhibitors of copper in sulfuric acid: combination of experimental and theoretical researches. *J. Taiwan Inst. Chem. Eng.* 106, 118–129.
- Ko, S.J., Choi, S.R., Hong, M.S., Kim, W.C., Kim, J.G., 2021. Effect of Imidazole as Corrosion Inhibitor on Carbon Steel Weldment in District Heating Water. *Materials* 14 (16), 4416.
- Srivastava, V., Salman, M., Chauhan, D.S., Abdel-Azeim, S., Quraishi, M.A., 2021. (E)-2-styryl-1H-benzo [d] imidazole as novel green corrosion inhibitor for carbon steel: Experimental and computational approach. *J. Mol. Liq.* 324.
- Wang, J., Singh, A., Talha, M., Luo, X., Deng, X., Lin, Y., 2018. Electrochemical and theoretical study of imidazole derivative as effective corrosion inhibitor for aluminium. *Int. J. Electrochem. Sci.* 13, 11539–11548.
- Xiong, S., Wu, H., Liu, Z., Wang, Y., Lin, W., 2021. Study on corrosion behavior of new corrosion inhibitor imidazole derivatives for mild steel in oil-in-water emulsion. *Surf. Interface Anal.* 53 (4), 418–431.
- Eduok, U., Ohaeri, E., Szpunar, J., 2018. Electrochemical and surface analyses of X70 steel corrosion in simulated acid pickling medium: Effect of poly (N-vinyl imidazole) grafted carboxymethyl chitosan additive. *Electrochim. Acta* 278, 302–312.
- Singh, A., Ansari, K.R., Kumar, A., Liu, W., Songsong, C., Lin, Y., 2017. Electrochemical, surface and quantum chemical studies of novel imidazole derivatives as corrosion inhibitors for J55 steel in sweet corrosive environment. *J. Alloys Compd.* 712, 121–133.
- Li, M., Ouyang, Y., Yang, W., Chen, Y., Zhang, K., Zuo, Z., Yin, X., Liu, Y., 2021. Inhibition performances of imidazole derivatives with increasing fluorine atom contents in anions against carbon steel corrosion in 1 M HCl. *J. Mol. Liq.* 322.
- Zeng, X., Zheng, X., Guo, L., Xu, Q., Huang, H., Tan, B., 2021. Three imidazole ionic liquids as green and eco-friendly corrosion inhibitors for mild steel in sulfuric acid medium. *J. Mol. Liq.* 324.
- Onyeachu, I.B., Njoku, D.I., Kaya, S., El Ibrahim, B., Nnadozie, C. F., 2021. Sour corrosion of C1018 carbon steel and its inhibition by 1-benzylimidazole: electrochemical, SEM, FTIR and computational assessment. *J. Adhes. Sci. Technol.*, 1–21 <https://doi.org/10.1080/01694243.2021.1938474>.
- Hachula, B., Nowak, M., Kusz, J., 2010. Crystal and molecular structure analysis of 2-methylimidazole. *J. Chem. Crystallogr.* 40, 201–206.
- Khahnadideh, S., Rezaei, Z., Khalafi-Nezhad, A., Bahrinajafi, A.R., Mohamadi, R., Farrokhrooz, A.A., 2003. Synthesis of N-Alkylated derivatives of imidazole as antibacterial agents, *Bioorganic. Med. Chem.* 13 (17), 2863–2865.
- 1-benzylimidazole, Material Safety Data Sheet, Cayman Chemicals, www.caymanchem.com/msds/70510m.pdf (Retrieved 30 October, 2021).
- Ismail, A., Irshad, H.M., Zeino, A., Torr, I.H., 2019. Electrochemical corrosion performance of aromatic functionalized imidazole inhibitor under hydrodynamic conditions on API X65 carbon steel in 1M HCl Solution. *Arab. J. Sci. Eng.* 44, 5877–5888.
- Solomon, M.M., Umoren, S.A., Quraishi, M.A., Tripathy, D.B., Abai, E.J., 2020. Effect of alkyl chain length, flow, and temperature on the corrosion inhibition of carbon steel in a simulated acidizing environment by an imidazole-based inhibitor. *J. Petrol. Sci. Eng.* 187.
- Umoren, S.A., Solomon, M.M., 2014. Effect of halide ions on the corrosion inhibition efficiency of different organic species—a review. *J. Ind. Eng. Chem.* 21, 81–100.
- Cardona, C., Narváez, L., Miranda, J.M., Acosta, A., 2014. Benzimidazole and Imidazole as Corrosion Inhibitors of AISI 316L Stainless Steel in Sulphuric Acid Medium, In ECS Meeting Abstracts No. 13 766. IOP Publishing.
- Ribeiro, J., Moreira, R.R., Soares, T.F., 2015. Electrochemical Impedance Spectroscopy Investigations of Stainless Steels in Presence of Corrosion Inhibitors, In ECS Meeting Abstracts No. 12 1079. IOP Publishing.
- Moreira, R.R., Soares, T.F., Ribeiro, J., 2014. Electrochemical investigation of corrosion on AISI 316 stainless steel and AISI 1010 carbon steel: study of the behaviour of imidazole and benzimidazole as corrosion inhibitors. *Adv. Chem. Eng. Sci.* 4, 503.
- Jia, M.Z., Zhang, Z., Ruan, L., Wu, F.M., 2013. Corrosion Inhibition Action of Imidazole Derivatives Self-assembled Films for 316 Stainless Steel. *J. Surf. Technol.* 42 (3), 23–27.
- ASTM-G 01–03, Standard practice for preparing, cleaning, and evaluation corrosion test specimens, ASTM Book of Standards (Re-approved 1997).
- Daniyal, M., Akhtar, S., 2020. Corrosion assessment and control techniques for reinforced concrete structures: a review. *J. Build. Pathol. Rehabil.* 5 (1), 1–20.
- Elgrishi, N., Rountree, K.J., McCarthy, B.D., Rountree, E.S., Eisenhart, T.T., Dempsey, J.L., 2018. A practical beginner's guide to cyclic voltammetry. *J. Chem. Edu.* 95 (2), 197–206.
- Strehblow, H.H., 2016. Passivity of metals studied by surface analytical methods, a review. *Electrochim. Acta* 212, 630–648.
- Maurice, V., Marcus, P., 2018. Progress in corrosion science at atomic and nanometric scales. *Prog. Mater. Sci.* 95, 132–171.
- Marcus, P., 1998. Surface science approach of corrosion phenomena. *Electrochim. Acta* 43, 109–118.
- Marcus, P., Maurice, V., Strehblow, H.H., 2008. Localized corrosion (pitting): A model of passivity breakdown including the role of the oxide layer nanostructure. *Corros. Sci.* 50, 2698–2704.
- Foad, E.E., 1999. El Sherbini, Effect of some ethoxylated fatty acids on the corrosion behaviour of mild steel in sulphuric acid solution. *Mater. Chem. Phys.* 60, 286–290.
- Onyeachu, I.B., Solomon, M.M., 2020. Benzotriazole derivative as an effective corrosion inhibitor for low carbon steel in 1 M HCl and 1 M HCl + 3.5wt.% NaCl solutions. *J. Mol. Liq.* 313.
- Onyeachu, I.B., Chauhan, D.S., Quraishi, M.A., Obot, I.B., Singh, A., 2021. (E)-2-amino-7-hydroxy-4-styrylquinoline-3-carbonitrile as a novel inhibitor for oil and gas industry: influence of temperature and synergistic agent. *J. Adhes. Sci. Technol.* <https://doi.org/10.1080/01694243.2021.1987100>.
- Umoren, S.A., Solomon, M.M., Udoso, I.I., Udoh, A.P., 2010. Synergistic and antagonistic effects between halide ions and carboxymethyl cellulose for the corrosion inhibition of mild steel in sulfuric acid solution. *Cellulose* 17, 635–648.
- Aramaki, K., Hackerman, N., 1969. Inhibition Mechanism of Medium-Sized Polymethyleneimine. *J. Electrochem. Soc.* 116 (5), 568.
- Mouheddin, T.A., Umoren, S.A., Obot, I.B., Ali, S.A., Solomon, M. M., 2019. Studies of the anticorrosion property of a newly synthesized Green isoxazolidine for API 5L X60 steel in acid environment. *J. Mater. Res. Technol.* 8 (5), 4399–4416.
- Mouheddin, T.A., Umoren, S.A., Obot, I.B., Ali, S.A., 2018. Isoxazolidine derivatives as corrosion inhibitors for low carbon steel in HCl solution: experimental, theoretical and effect of KI studies. *RSC Adv.* 8, 1764–1777.

- Akinbulumo, O.A., Odejebi, O.J., Odekanle, E.L., 2020. Thermodynamics and adsorption study of the corrosion inhibition of mild steel by *Euphorbia heterophylla* L. extract in 1.5 M HCl. *Results Mater.* 5.
- Chaudhary, S., Tak, R.K., 2022. Natural corrosion inhibition and adsorption characteristics of *Tribulus terrestris* plant extract on aluminium in hydrochloric acid environment. *Biointerface Res. Appl. Chem.* 12 (2), 2603–2617.
- Hsu, C.H., Mansfeld, F., 2001. Technical note: concerning the conversion of the constant phase element parameter Y_0 into a capacitance. *Corros.* 57, 747.
- Shoesmith, D.W., Taylor, P., Bailey, M.G., Owen, D.G., 1980. The formation of ferrous monosulfide polymorphs during the corrosion of iron by aqueous hydrogen sulfide at 21 °C. *J. Electrochem. Soc.* 127 (5), 1007–1015.
- Deen, K.M., Lodhi, M.J.K., Asselin, E., Haider, W., 2020. Charge Transport Characteristics of the Passive Oxide Film Formed on 3D Printed 316 L Stainless Steel in the Presence of FeII/FeIII Species. *J. Phys. Chem. C* 124, 21435–21445.
- Tang, J., Yang, X., Wang, Y., Wang, H., Xiao, Y., Apreutesei, M., Nie, Z., Normand, B., 2019. Corrosion Behavior of 2205 Duplex Stainless Steels in HCl Solution Containing Sulfide. *Metals* 9, 294.
- Onyeachu, I.B., Obot, I.B., Sorour, A.A., Abdul-Rashid, M.I., 2019. Green corrosion inhibitor for oilfield application I: Electrochemical assessment of 2-(2-pyridyl) benzimidazole for API X60 Steel under sweet environment in NACE brine ID196. *Corros. Sci.* 150, 183–193.
- Tait, W.S., 2018. *Electrochemical corrosion basics Handbook of Environ. Degrad. Mater.* Third Ed. (Amsterdam: Elsevier Inc) 97–115.
- Esmailzadeh, S., Aliofkhaezai, M., Sarlak, H., 2018. Interpretation of cyclic potentiodynamic polarization test results for study of corrosion behavior of metals: A Review. *Prot. Met. Phys. Chem. Surf.* 54, 976–989.
- Moravcik, I., Peighambardoust, N.S., Motallebzadeh, A., Moravcikova-Gouvea, L., Liu, C., Prabhakar, J.M., Dlouhy, I., Li, Z., 2021. Interstitial nitrogen enhances corrosion resistance of an equiatomic CoCrNi medium-entropy alloy in sulfuric acid solution. *Mater. Charact.* 172.
- Loto, R.T., Solomon, M.M., 2021. Corrosion resistance and passivation behavior of 3004 AlMnMg and 4044AlSi aluminum alloys in acid-chloride electrolytes. *Mater. Res. Express* 8.
- Ait Albrimi, Y., Eddib, A., Douch, J., Berghoute, Y., Hamdani, M., Souto, R.M., 2011. Electrochemical Behaviour of AISI 316 Austenitic Stainless Steel in Acidic Media Containing Chloride Ions. *Int. J. Electrochem. Sci.* 6, 4614–4627.
- Mulimbayan, F.M., Mena, M.G., 2016. Cyclic voltammetric study of the pitting corrosion behavior of low-nickel austenitic stainless steels in citric acid. *Mater. Sci. Forum* 866, 191–195.
- Knapp, Q.W., Wren, J.C., 2012. Film formation on type-316L stainless steel as a function of potential: Probing the role of gamma-radiation. *Electrochim. Acta* 80, 90–99.
- Onyeachu, I.B., Obot, I.B., Alamri, A., Eziukwu, C.A., 2020. Effective acid corrosion inhibitors for X60 steel under turbulent flow conditions based on benzimidazoles: Experimental, theoretical, SEM, ATR-IR and XPS investigations. *Eur. Phys. J. Plus* 135, 129.
- Abdallah, M., 2002. Rhodanine azosulpha drugs as corrosion inhibitors for corrosion of 304 stainless steel in hydrochloric acid solution. *Corr. Sci.* 44, 717–728.
- Scendo, M., Trela, J., 2013. Adenine as an effective corrosion inhibitor for stainless steel in chloride solution. *Int. J. Electrochem. Sci.* 8, 9201–9221.
- Asfia, M.P., Rezaei, M., Bahlakeh, G., 2020. Corrosion prevention of AISI 304 stainless steel in hydrochloric acid medium using garlic extract as a green corrosion inhibitor: electrochemical and theoretical studies. *J. Mol. Liq.* 315.
- Koumya, Y., Idouhli, R., Oukhri, A., Khadiri, M., Abouelfida, A., Benyaich, A., 2020. Synthesis, Electrochemical, Thermodynamic, and Quantum Chemical Investigations of Amino Cadalene as a Corrosion Inhibitor for Stainless Steel Type 321 in Sulfuric Acid 1M. *Int. J. Electrochem.* 10, 1–10.
- Matos, L.A.C., Taborda, M.C., Alves, G.J.T., da Cunha, M.T., do Prado Banczek, E., De Fátima Oliveira, M., Delia, E., Rodrigues, P.R.P., 2018. Application of an Acid Extract of Barley Agro-Industrial Waste as a Corrosion Inhibitor for Stainless Steel AISI 304 in H₂SO₄. *Int. J. Electrochem. Sci.* 13, 1577–1593.
- Sanni, O., Popoola, A.P.I., Fayomi, O.S.I., 2019. Temperature Effect, Activation Energies and Adsorption Studies of Waste Material as Stainless Steel Corrosion Inhibitor in Sulphuric Acid 0.5 M. *J. Bio-Tribo-Corros.* 5, 88.
- Fouda, A.S., Abd El-Maksoud, S.A., Belal, A.A.M., El-Hossiany, A., Ibrahim, A., 2018. Effectiveness of Some Organic Compounds as Corrosion Inhibitors for Stainless Steel 201 in 1M HCl: Experimental and Theoretical Studies. *Int. J. Electrochem. Sci.* 13, 9826–9846.
- Mazkour, A., El Hajjaji, S., Labjar, N., El Mostapha, L., El Mahi, M., 2021. Corrosion Inhibition Effect of 5-Azidomethyl-8- Hydroxyquinoline on AISI 321 Stainless Steel in Phosphoric Acid Solution. *Int. J. Electrochem. Sci.* 16.